ACS OMEGA

http://pubs.acs.org/journal/acsodf

Article

Configuration Analysis of a Lizard Skin-like Pattern Formed by DNA Self-Assembly

Anshula Tandon,[§] Muhammad Tayyab Raza,[§] Suyoun Park, Sungjin Lee, Thi Bich Ngoc Nguyen, Thi Hong Nhung Vu, Seungjae Kim, Tai Hwan Ha,* and Sung Ha Park*

Cite This: *ACS Omega* 2021, 6, 27038−27044

Read Online

ACCESS | Metrics & More | Article Recommendations | Supporting Information

ABSTRACT: Nature manifests diverse and complicated patterns through efficient physical, chemical, and biological processes. One of the approaches to generate complex patterns, as well as simple patterns, is the use of the cellular automata algorithm. However, there are certain limitations to produce such patterns experimentally due to the difficulty of finding candidate programmable building blocks. Here, we demonstrated the feasibility of generating an ocellated lizard skin-like pattern by simulation considering the probabilistic occurrence of cells and constructed the simulation results on DNA lattices via bottom-up self-assembly. To understand the similarity between the simulated pattern (SP) and the observed pattern (OP) of lizard skin, a unique configuration scheme (unit configuration was composed of 7 cells) was conceived. SPs were generated through a computer with a controlling population of gray and black cells in a given pattern. Experimental patterns (EPs) on DNA lattices, consisting of double-crossover (DX) tiles without and with protruding hairpins, were fabricated and verified through atomic force microscopy (AFM). For analyzing the similarity of the patterns, we introduced deviation of the average configuration occurrence for SP and EP with respect to OP, i.e., σ_α(SO) and σ_α(EO). The configuration and deviation provide characteristic information of patterns. We recognized that the minimum values of $<\sigma_\alpha(\mathrm{SO})>$ and $<\sigma_\alpha(\mathrm{EO})>$ occurred when 50% (55%) of black cells in given SPs (DX tiles with hairpins in given EPs) appeared to be most similar to the OP. Our study provides a novel platform for the applicability of DNA molecules to systematically demonstrate other naturally existing complex patterns or processes with ease.

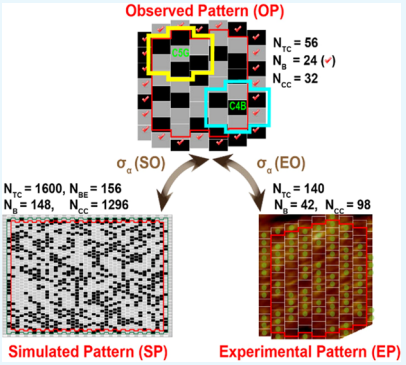

INTRODUCTION

Attributable to biocompatibility (in biotechnology) and structural stability (in nanotechnology), DNA molecules have emerged as particularly promising biomaterials for a versatile building block. Structural DNA nanotechnology (which provides methods to fabricate various dimensional nanostructures with periodic and aperiodic patterns formed by self-assembly) is significantly developed by sequence programmability (information technology) via Watson−Crick base-pairing interactions.[1−12] Self-assembly is an efficient way to produce thermodynamically favored patterns at the nanoscale through noncovalent interaction with precisely controlled topology.[13]

Nature, an inexhaustible source, manifests diverse patterns with remarkable structures produced through efficient chemical processes. These patterns can be considered as the set of dynamic organizing principles and can be explained by the interdisciplinary fields of physics, chemistry, mathematics, and biology. A commonly used approach to study the formation of these patterns is computer modeling to simulate a wide range of natural phenomena.[14−23] Recently, Milinkovitch's group studied an ocellated lizard by observation (via scale color dynamics) and simulation (a discrete-state dynamical lattice of mesoscopic elements) of labyrinthine skin pattern.[24] The general rule was that black cells tend to have four gray neighbors and gray cells tend to have three black neighbors. Thus, it was proposed that the lizard skin color pattern was superposed on the skin cells because of the superposition of skin geometry with a continuous reaction−diffusion system.

To date, naturally occurring patterns (such as lizard skin-like and Zelkova serrata lenticel-like patterns), which do not have specific known rules, are seldom demonstrated experimentally. Even if so, quantitative analysis of the similarity between an observed pattern (OP) and an experimentally obtained pattern is rarely discussed. In this study, we tested the feasibility to generate a lizard skin-like pattern by simulation with the aid of the probabilistic occurrence of cells and constructed the simulation results on DNA lattices via bottom-up self-assembly. To analyze the similarity between the simulated pattern (SP) or experimental pattern (EP) and the observed

Received: July 8, 2021
Accepted: September 21, 2021
Published: October 5, 2021

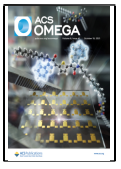

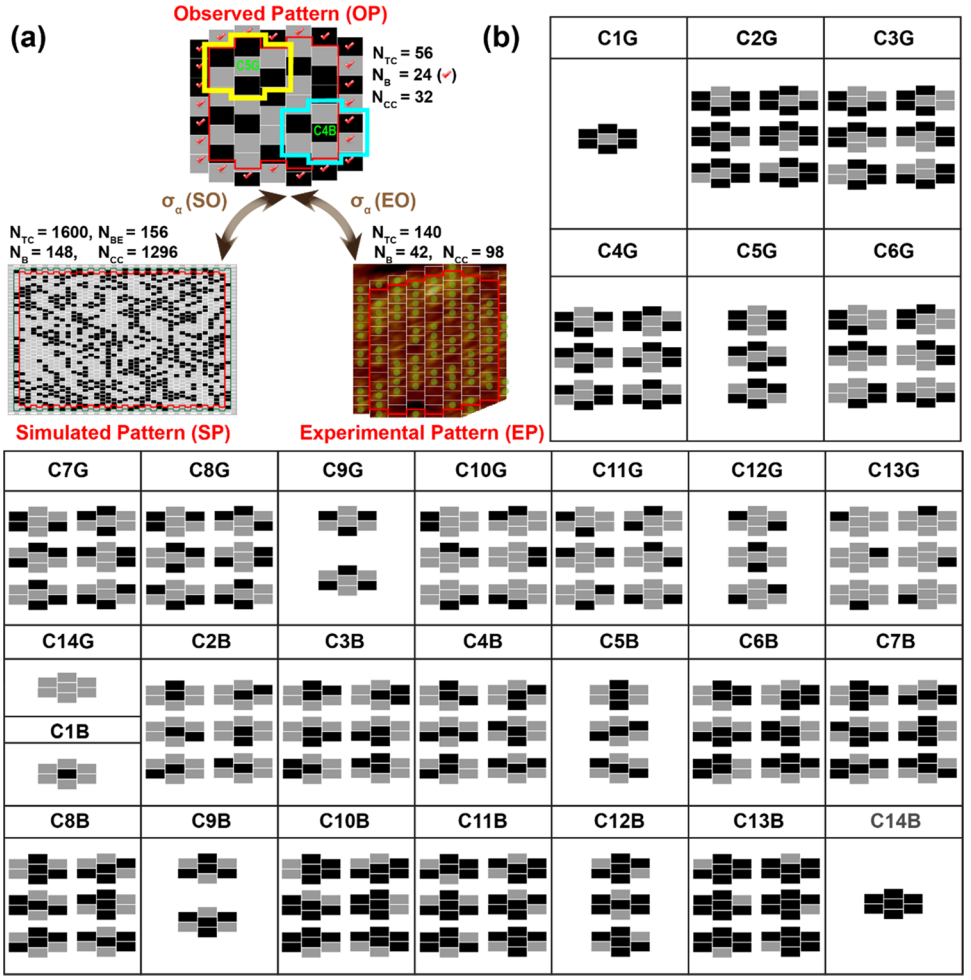

Figure 1. Demonstration of simulated patterns (SPs) and experimental patterns (EPs) with respect to the observed pattern (OP) of the lizard skin and a list of all available configurations. (a) Representative OP, SP, and EP. The total number of cells, empty boundary cells, boundary cells, and the number of cells providing countable configurations in given lattices are abbreviated as N_{TC}, N_{BE}, N_B, and N_{CC}, respectively. Boundary lines (an empty boundary line) in OP, SP, and EP (SP) are indicated in red (green). Twenty-four cells of N_B in OP are indicated with red checkmarks. A configuration unit consists of 7 cells, such as C5G (shown by the yellow line) and C4B (cyan) in the OP. EP was formed by DNA DX tiles without and with protruding hairpins. Green dots in EP indicate DX tiles having hairpins. The deviation of configuration occurrence is represented by σ_α. Here, σ_α(SO) and σ_α(EO) stand for the deviation of SP with respect to OP and the deviation of EP with respect to OP, respectively. (b) Schematic representation of all possible configurations. Twenty-eight configurations (i.e., 14 for a mid-gray cell and another 14 for a mid-black) are available.

pattern (OP) of the lizard skin (we adopted OP from ocellated lizards[24]), countable configuration (units consisting of 7 cells) was introduced. EPs on DNA lattices, which were composed of double-crossover (DX) tiles without and with protruding hairpins, were constructed and verified through atomic force microscopy (AFM).[2] To explain the similarity between the patterns, we introduced the deviation of average configuration occurrence (α) for SP and EP with respect to OP (i.e., σ_α(SO) and σ_α(EO)).

RESULTS AND DISCUSSION

Discussion of OP, SP, and EP of the Lizard Skin and a List of Available Configurations. Figure 1a depicts representative patterns obtained from simulation (SP, which is generated through a computer by controlling the number of black cells in given countable configurations), experiment (EP, which consists of carefully designed DNA DX tiles formed via bottom-up self-assembly), and observation (OP) with the specific numbers of the cells and the deviations (σ_α) of configuration occurrence (α). The total number of cells, boundary cells, and cells providing countable configurations in given lattices are named N_{TC}, N_B, and N_{CC}, respectively. For OP and EP, boundary lines are indicated in red. Twenty-four N_B cells in OP (total number of cells placed outside of the boundary line) are indicated with red checkmarks. Here, the sum of N_B and N_{CC} is N_{TC}. For instance, 32 of N_{CC} is obtained by subtraction of 24 of N_B from 56 of N_{TC} for OP. For SP, we introduced an empty boundary line, which is indicated in green (for programming purposes). The total number of cells placed outside of the empty boundary line is named N_{BE}. Consequently, N_{TC} is given by the sum of N_B, N_{BE}, and N_{CC}.

Configuration and deviation provide characteristic information of patterns. A configuration unit consists of 7 cells. A mid rectangular cell (either gray or black) with its 6 neighboring cells forms a unit of hexagonal countable configuration. Here, C5G (shown by a yellow line) and C4B (cyan) in OP indicate a 5th configuration having a mid-gray cell and a 4th configuration having a mid-black cell, respectively. Each cell in a unit can be either gray or black, which corresponds to without or with protruding hairpins on DNA DX tiles, respectively. For clarity, we placed green dots in EP (obtained

https://doi.org/10.1021/acsomega.1c03593
ACS Omega 2021, 6, 27038−27044

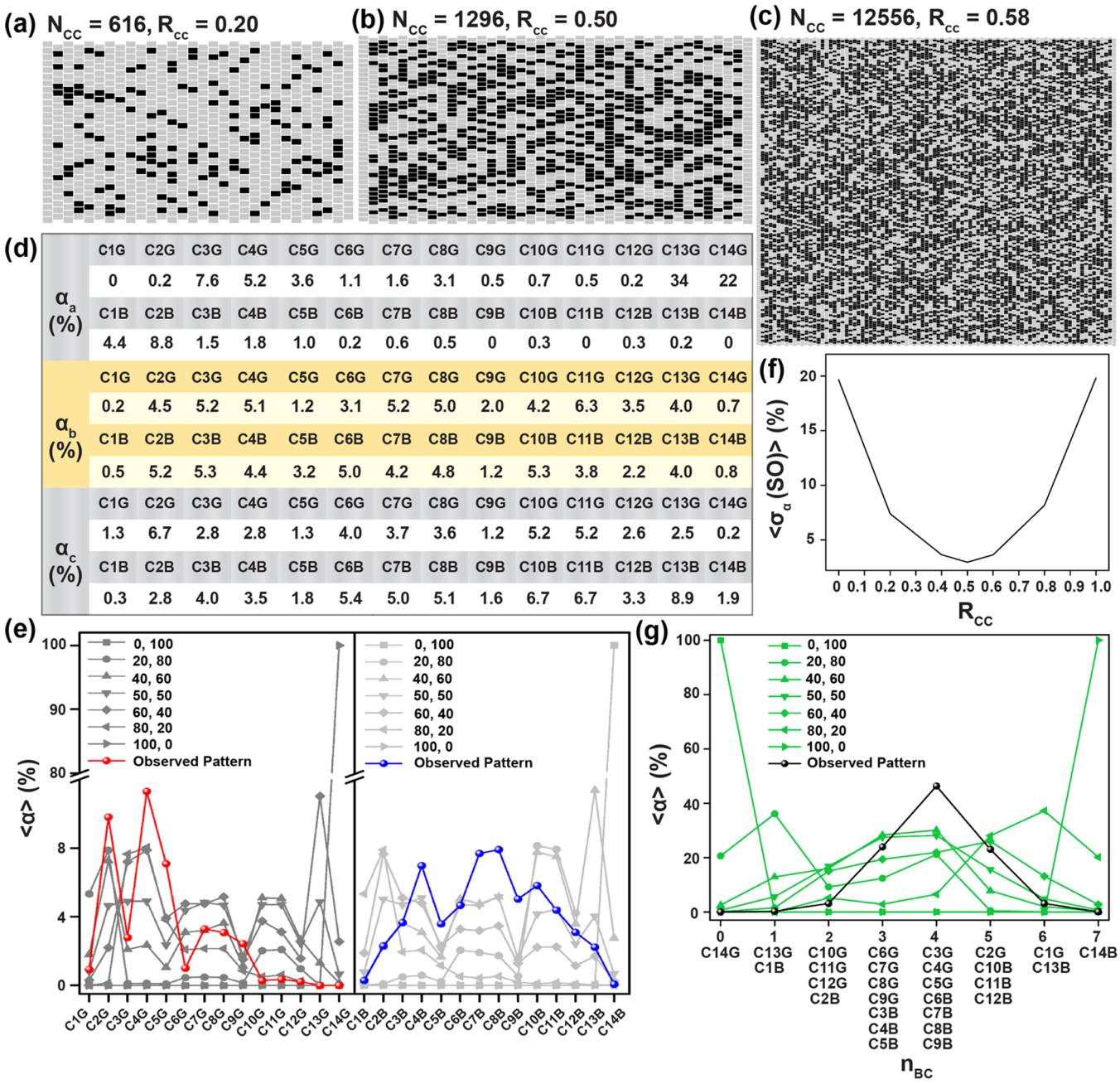

Figure 2. Demonstration and analysis of simulated patterns (SPs) with respect to the observed pattern (OP) of the lizard skin. (a) Representative SP with a lattice size of 24 × 26 cells. R_{CC} is defined as the ratio of the number of black cells in given countable configurations ($N_{CC,B}$) over the number of cells providing the countable configurations (N_{CC}), i.e., $R_{CC} = N_{CC,B}/N_{CC}$. A lattice shown here has an R_{CC} of 0.2. (b, c) Representative SPs with lattice sizes of 36 × 36 and 146 × 86 cells. (d) Configuration occurrences (named α_a, α_b, and α_c) for lattices shown in (a), (b), and (c). (e) Average configuration occurrences (<α>) for SPs with a lattice size of 146 × 86 cells. Fifty SPs were evaluated. SPs are labeled with the percentage ratio of the number of black ($N_{CC,B}$) and gray ($N_{CC,G}$) cells in given countable configurations. Configuration occurrences for OP are indicated with red (for mid-gray cells) and blue (for mid-black cells) lines. (f) Deviation of average configuration occurrences (σ_α) for SPs with a lattice size of 146 × 86 cells. (g) <α> with respect to the number of black cells within a given configuration. The number of black cells within countable configurations is named n_{BC}. Specific names of corresponding configurations are listed under n_{BC}. <α> for OP is marked with a black line.

from an AFM image), which indicate cells (i.e., DX tiles) having hairpins. To determine the similarity between patterns, we introduced the deviation of configuration occurrence (α), which is represented by σ_α. Here, σ_α(SO) and σ_α(EO) indicate the deviation of SP with respect to OP and the deviation of EP with respect to OP, respectively.

Figure 1b shows a schematic representation of all possible configurations. Twenty-eight configurations (i.e., 14 for a mid-gray cell and another 14 for a mid-black) are available. Each configuration has either 1, 2, 3, or 6 units depending upon the characteristics of the configuration. For instance, C1G (C1B), which is the 1st configuration having a mid-gray (black) cell with all neighboring black (gray) cells, requires only 1 unit. In contrast, C10G (C10B) having a mid-gray (black) cell needs 6 units to construct 2 adjacent black (gray) cells in 6 neighboring cells.

Demonstration and Analysis of SPs with Respect to the OP of the Lizard Skin. Figure 2 demonstrates the SPs of

https://doi.org/10.1021/acsomega.1c03593
ACS Omega 2021, 6, 27038−27044

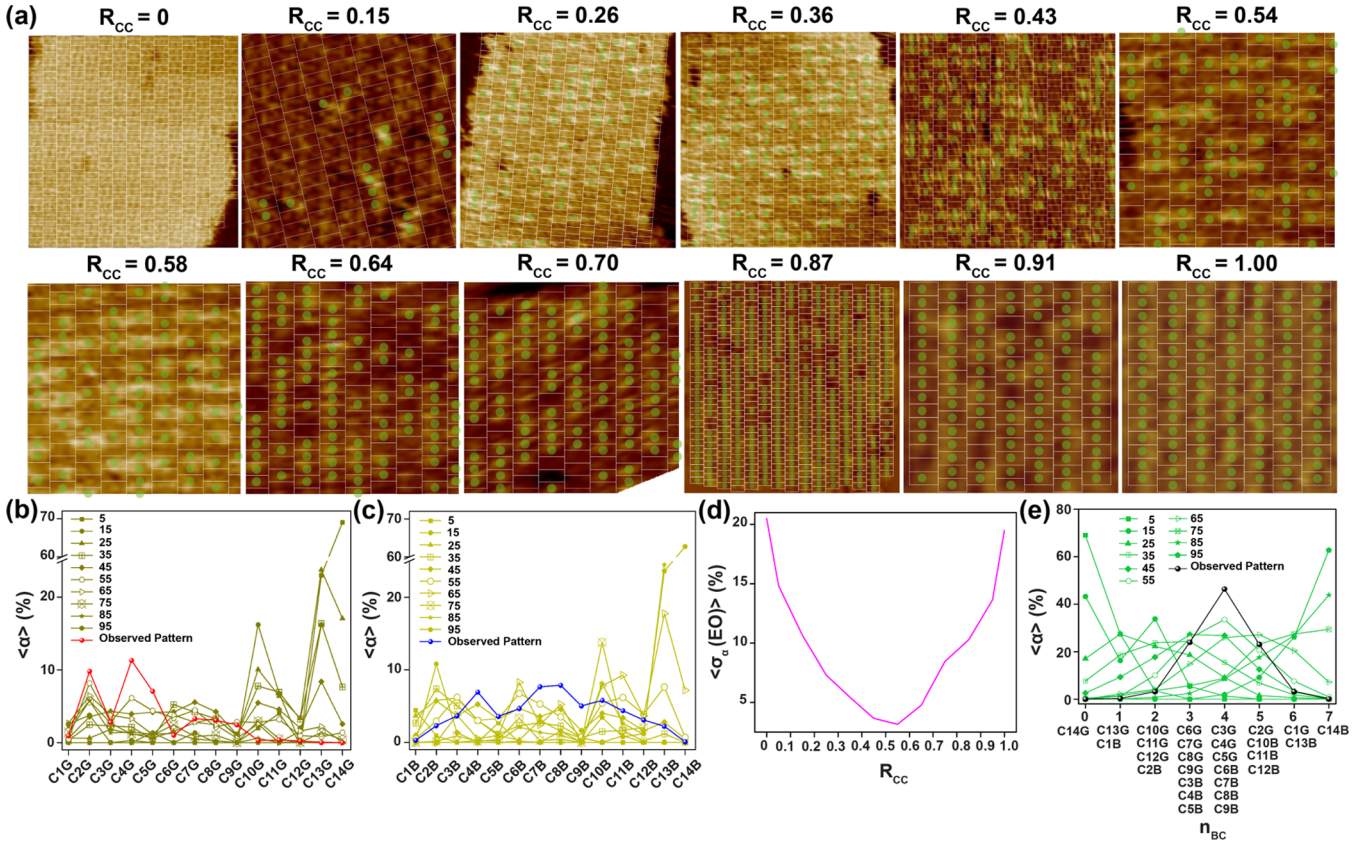

Figure 3. Demonstration and analysis of experimental patterns (EPs) with respect to the observed pattern (OP) of the lizard skin. (a) Representative EPs with various values of R_{CC} obtained by AFM data. Green dots in EP indicate cells having hairpins. AFM images for R_{CC} values of 0, 0.26, 0.36, 0.43, and 0.87 had a scan size of 200 × 200 nm^2, while the scan size of all others was 100 × 100 nm^2. (b, c) Average configuration occurrences (<α>) for EPs. EPs are labeled with the mid values of R_{CC}. For instance, 25 indicates EPs with a range of R_{CC} between 21 and 30. Configuration occurrences for OP are indicated with red (for mid-gray cells) and blue (for mid-black cells) lines. (d) Deviation of average configuration occurrences (σ_α) for EPs with various values of R_{CC}. (e) <α> with respect to the number of cells with hairpins within a given configuration. The number of cells with hairpins within countable configurations is named n_{BC}. <α> for OP is marked with a black line.

the lizard skin [which are generated through one-dimensional (1D) cellular automata]. Three representative SPs (with lattice sizes of 24 × 26, 36 × 36, and 146 × 86 cells) corresponding to N_{CC} values of 616, 1296, and 12 556 are displayed in Figure 2a−c. To generate diverse SPs, we introduced R_{CC}, which is defined as the ratio of the number of black cells in given countable configurations ($N_{CC,B}$) to the number of cells providing countable configurations (N_{CC}) (i.e., $R_{CC} = N_{CC,B}/N_{CC}$). For instance, the 2nd and 3rd SPs shown here have R_{CC} values of 0.5 (=648/1296) and 0.58 (=7283/12556), respectively. As the R_{CC} value increases, the number of black cells in a given SP increases.

Numerical values of configuration occurrences for given SPs, named as α_a, α_b, and α_c (shown in Figure 2a−c) are noticed in Figure 2d. We obtained $\alpha_{C\#G(B)}$ by $(N_{CC,C\#G(B)}/N_{CC}) \times 100$. Here, $N_{CC,C\#G(B)}$ stands for the number of C#G(B) configuration occurrences. For instance, the proportion of $\alpha_{a,C2B}$ and $\alpha_{c,C7G}$ compared to other configurations is 8.8% [obtained by $(N_{CC,C2B}/N_{CC}) \times 100 = (54/616) \times 100$] and 3.7% [$(N_{CC,C7G}/N_{CC}) \times 100 = (465/12556) \times 100$], respectively. As can be seen, the most dominant configuration for the 1st SP was the C13G (the 13th configuration having a mid-gray cell and 1 black and 5 gray neighboring cells) with 34.0% of configuration occurrences being $\alpha_{a,C13G}$, and the least dominant configuration for the 2nd SP was C1G (the 1st configuration having a mid-gray cell and all black neighboring cells), with $\alpha_{b,C1G}$ representing 0.2% of configuration occurrences. Similarly, the most and least dominant configurations for the 3rd SP were C13B, with 8.9% of $\alpha_{c,C13B}$, and C14G, with 0.2% of $\alpha_{c,C14G}$, respectively.

For obtaining the average configuration occurrence (<α>) for SPs with various R_{CC} values, we evaluated 50 SPs having a lattice size of 146 × 86 cells for each R_{CC} (Figure 2e). SPs were labeled with the ratio of the number of black ($N_{CC,B}$) to gray ($N_{CC,G}$) cells in given countable configurations. For example, 20 in (20, 80) indicates $R_{CC} \times 100$. It means that SPs labeled with (20, 80), (50, 50), and (100, 0) have an R_{CC} of 0.20, 0.50, and 1.00, respectively. Configuration occurrence percentages for OP are indicated with red lines for mid-gray cells and blue lines for mid-black cells. For countable configurations with mid-gray cells (C#G, left panel), OP reveals dominant <α> occurred at C4G (11.0%) followed by C2G (8%). However, in SPs, the most occurred configurations are C2G (7.9%) for (20, 80), C2G (7.3%) for (40, 60), C13G (11%) for (60, 40), and C13G (31%) for (80, 20). In contrast, the dominant <α>, with a roughly constant value (4.5%), is obtained at several configurations such as C2G, C3G, C4G, C6G, C7G, C8G, C10G, C11G, and C13G for (50, 50). The right panel in Figure 2e displays a plot of <α> against the 14 configurations having mid-black cells (C#B). OP reveals two dominant <α> occurred at C7B (8%) and C8B (8%). In SP, most the occurred <α> are C13B (32%) for (20,80), C13B (11%) for

https://doi.org/10.1021/acsomega.1c03593
ACS Omega 2021, 6, 27038−27044

(40, 60), C2B (8%) for (60, 40), and C2B (8%) for (80, 20). For (50, 50), <α> of C2B, C3B, C4B, C6B, C7B, C8B, C10B, C11B and C13B are placed in the range of 4−5%.

Figure 2f displays a plot of the average deviation of configuration occurrence (<σ_α(SO)>) for SPs with respect to OP. It is defined by $<\sigma_\alpha(\mathrm{SO})> = [\sum(\alpha_i - <\alpha_i>)^2/(N-1)]^{1/2}$, where α_i, $<\alpha_i>$, and N represent average configuration occurrence of SP and OP at the i^{th} configuration and the total number of available configurations (i.e., 28), respectively. We recognize that <σ_α(SO)> shows a minimum (3.0%) at R_{CC} = 0.50. This means that SP with an R_{CC} of 0.50 provides the most similar configuration to OP than any other samples quantitatively.

<α> with respect to the number of black cells within a given configuration is displayed in Figure 2g. The number of black cells within a countable configuration (from 0 to 7) is named as n_{BC}. Specific names of corresponding configurations are listed under n_{BC}. For instance, configurations of C10G, C11G, C12G, and C2B have 2 black cells within the unit configuration placed under an n_{BC} of 2. For OP, <α> is marked with a black line. Furthermore, for OP, <α> is found to be highest (46%) at an n_{BC} of 4. The highest <α> for SPs with (20,80), (40,60), (50,50), (60,40), and (80,20) were calculated as 36, 30, 28, 26, and 37%, respectively.

Demonstration and Analysis of EPs with Respect to the OP of the Lizard Skin. Figure 3a illustrates representative EPs obtained by AFM data with various values of R_{CC}. For better visualization, AFM images are overlaid with rectangular boxes representing DX tiles. Green dots in EPs indicate cells (i.e., DX tiles) having hairpins. A DX tile (with dimensions of 12.6 × 4 nm^2) is formed by hybridization followed by facilitating further assembly into EPs. To represent the mid-black (gray) cells in OPs, DX tiles with (without) hairpins are employed. For obtaining various EPs, EPs having different R_{CC} values are fabricated by controlling the ratio of the number of DX tiles with hairpins to the total number of DX tiles in a given EP. Average configuration occurrences (<α>) for EPs are shown in Figure 3b,c. Configuration occurrences for OP are indicated with red (indicating mid-gray cells) and blue (indicating mid-black cells) lines. EPs are labeled with the mid values of R_{CC}. For instance, 45 indicates EPs with a range of R_{CC} between 41 and 50. For mid-gray (black) configurations in OPs, C4G (C7B and C8B) is (are) more dominant than others. For mid-gray (black) configurations in EPs, the most occurred configurations among <α> are C14G (C1B) for 5% of R_{CC}, C14G (C2B) for 15%, C13G (C2B) for 25%, C13G (C3B) for 35%, C13G (C2B) for 45%, C2G (C13B) for 55%, C2G (C13B) for 65%, C2G (C14B) for 75%, C2G (C14B) for 85%, and C2G (C14B) for 95%.

The deviation of average configuration occurrences (σ_α) for EPs as a function of R_{CC} is plotted and shown in Figure 3d. The minimum of σ_α (i.e., 3.2%) occurs at an R_{CC} of 0.55. This might imply that 55% of DX tiles with hairpins in EPs appear to be most similar to the OP.

Figure 3e displays <α> with respect to the number of cells with hairpins within a given configuration. The number of cells with hairpins within countable configurations is named as n_{BC}. Specific names of corresponding configurations are listed under n_{BC} (e.g., configurations of C2G, C10B, C11B, and C12B have 5 cells with hairpins within the unit configuration and are placed under an n_{BC} of 5). A black line represents <α> for OP. In the case of OPs, <α> revealed its highest values at an n_{BC} of 4. In EPs, the highest <α> is occurred at an n_{BC} of 0 for 5% of R_{CC}, an n_{BC} of 0 for 15% of R_{CC}, an n_{BC} of 1 for 25% of R_{CC}, an n_{BC} of 2 for 35% of R_{CC}, an n_{BC} of 3 for 45% of R_{CC}, an n_{BC} of 4 for 55% of R_{CC}, an n_{BC} of 5 for 65% of R_{CC}, an n_{BC} of 7 for 75% of R_{CC}, an n_{BC} of 7 for 85% of R_{CC}, and an n_{BC} of 7 for 95% of R_{CC}.

Deviation of Average Configuration Occurrence for SPs and EPs with Respect to the OP of the Lizard Skin. To compare the similarity between SP (EP) and OP, <σ_α(SO)> and <σ_α(EO)> are plotted in Figure 4 as a function of R_{CC}.

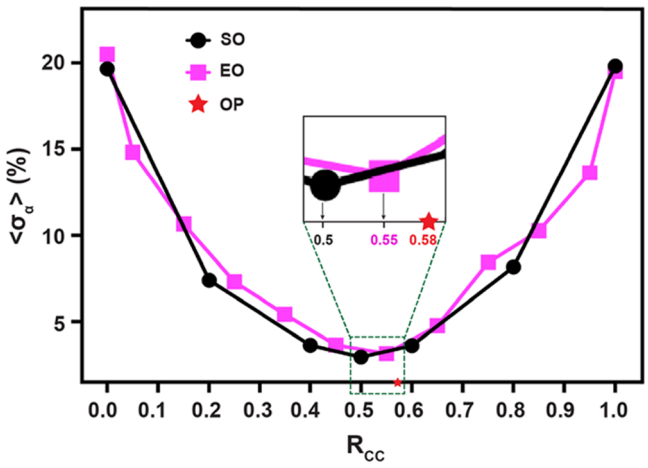

Figure 4. Deviation of average configuration occurrence (σ_α) for SP and EP with respect to OP, i.e., σ_α(SO) and σ_α(EO), as a function of R_{CC}. An enlarged image shows the minimum values of σ_α(SO) and σ_α(EO), which occurred at R_{CC} values of 0.50 and 0.55, respectively. R_{CC} of OP, which was 0.58, is marked with a red star.

By analyzing OPs, an R_{CC} of 0.58 was obtained (which is marked with a red star). Minimum values of <σ_α(SO)> and <σ_α(EO)> occurred at R_{CC} of 0.50 and 0.55, respectively. This might imply that 50% (55%) of black cells in given SPs (DX tiles with hairpins in given EPs) were most similar to the OP. In addition, we noticed that the R_{CC} of SP and EP agreed well with the R_{CC} of OP (=0.58) within 13.8% [=(|0.50−0.58|/0.58) × 100] and 5.2% deviations (indicated in an enlarged image).

CONCLUSIONS

In this study, we discussed how an observed lizard pattern could be generated experimentally as well as by simulation. In addition, we analyzed them through configuration analysis of a lizard skin-like pattern formed by simulation and DNA self-assembly. To generate diverse SPs and EPs, we introduced R_{CC} (which is defined as the ratio of the number of black cells in given countable configurations to the total number of cells providing countable configurations). As the R_{CC} increases, the number of black cells in given SPs and EPs increase. Numerical values of configuration occurrences (which heavily relied on R_{CC}) for given SPs and EPs were carefully examined. To obtain similarity between SP/EP and OP, we investigated <σ_α(SO)> and <σ_α(EO)> as a function of R_{CC}. The minima of <σ_α(SO)> and <σ_α(EO)> (which describe the most similar pattern to the OP) occurred at R_{CC} values of 0.50 and 0.55, respectively.

METHODS

Construction of the Experimental Patterns (EP) Formed by DNA Double-Crossover (DX) Tiles. Synthetic

https://doi.org/10.1021/acsomega.1c03593
ACS Omega 2021, 6, 27038−27044

oligonucleotides purified via high-performance liquid chromatography (HPLC) were purchased from Bioneer (Daejeon, Korea). For hybridization of the EPs, the two-step annealing method was adopted. Individual strands for each tile (i.e., R_0 and S_0 tiles having no hairpins and R_1 and S_1 strands with hairpins) were mixed with equimolar concentration (400 nM) in 1 × TAE/Mg^{2+} buffer solution (40 mM Tris, 20 mM acetic acid, 1 mM ethylenediaminetetraacetic acid (EDTA) [pH 8.0], and 12.5 mM magnesium acetate). For obtaining individual tiles, the mixture of individual strands for each tile in the test tube was cooled from 95 to 25 °C by placement in a Styrofoam box containing 2 L of boiled water for 2 days to facilitate the hybridization process (i.e., first step: high-temperature annealing). For construction of EPs with specific values of R_{cc}, R_0, S_0, and R_1, S_1 were mixed with appropriate concentrations of individual tiles. For instance, EPs with R_{cc} of 0, 0.2, 0.5, and 1.0 were formed by following sets: ($[R_0] = [S_0] = 100$ nM and $[R_1] = [S_1] = 0$ nM), ($[R_0] = [S_0] = 80$ nM and $[R_1] = [S_1] = 20$ nM), ($[R_0] = [S_0] = 50$ nM and $[R_1] = [S_1] = 50$ nM), and ($[R_0] = [S_0] = 0$ nM and $[R_1] = [S_1] = 100$ nM), respectively. Mixtures were then placed in 2 L of water in a Styrofoam box and gradually cooled down from 40 to 25 °C to facilitate further hybridization (second step: low-temperature annealing) (Supporting Information Figure S1, Supporting Information Tables S1 and S2).

AFM Imaging. DNA sample solution (5 μL) was dropped on a cleaved mica surface (with a size of 5 × 5 mm^2) followed by incubation for 30 s. Then, 30 μL of 1 × TAE/Mg^{2+} was added to mica and another 20 μL of 1 × TAE/Mg^{2+} was mounted on an oxide-sharpened silicon nitride AFM tip (Veeco, CA). AFM images were obtained in the scan-assist mode by a Digital Instruments Nanoscope V8 (Veeco, CA).

■ ASSOCIATED CONTENT

Supporting Information

The Supporting Information is available free of charge at https://pubs.acs.org/doi/10.1021/acsomega.1c03593.

Schematic illustration of DX tiles without (R_0, S_0) and with hairpins (R_1, S_1) with their detailed base sequences for EP formation, strand details representing the number of bases and DNA sequences used in DX tiles, and sequence of the sticky ends used in DX tiles (PDF)

■ AUTHOR INFORMATION

Corresponding Authors

Tai Hwan Ha − *Core Facility Management Center, Korea Research Institute of Bioscience and Biotechnology (KRIBB), Daejeon 34141, Korea;* orcid.org/0000-0003-0892-3320; Email: taihwan@kribb.re.kr

Sung Ha Park − *Department of Physics, Institute of Basic Science, and Sungkyunkwan Advanced Institute of Nanotechnology (SAINT), Sungkyunkwan University, Suwon 16419, Korea;* orcid.org/0000-0002-0256-3363; Email: sunghapark@skku.edu

Authors

Anshula Tandon − *Department of Physics, Institute of Basic Science, and Sungkyunkwan Advanced Institute of Nanotechnology (SAINT), Sungkyunkwan University, Suwon 16419, Korea*

Muhammad Tayyab Raza − *Department of Physics, Institute of Basic Science, and Sungkyunkwan Advanced Institute of Nanotechnology (SAINT), Sungkyunkwan University, Suwon 16419, Korea*

Suyoun Park − *Department of Physics, Institute of Basic Science, and Sungkyunkwan Advanced Institute of Nanotechnology (SAINT), Sungkyunkwan University, Suwon 16419, Korea*

Sungjin Lee − *Department of Physics, Institute of Basic Science, and Sungkyunkwan Advanced Institute of Nanotechnology (SAINT), Sungkyunkwan University, Suwon 16419, Korea*

Thi Bich Ngoc Nguyen − *Department of Physics, Institute of Basic Science, and Sungkyunkwan Advanced Institute of Nanotechnology (SAINT), Sungkyunkwan University, Suwon 16419, Korea*

Thi Hong Nhung Vu − *Department of Physics, Institute of Basic Science, and Sungkyunkwan Advanced Institute of Nanotechnology (SAINT), Sungkyunkwan University, Suwon 16419, Korea*

Seungjae Kim − *Department of Physics, Institute of Basic Science, and Sungkyunkwan Advanced Institute of Nanotechnology (SAINT), Sungkyunkwan University, Suwon 16419, Korea*

Complete contact information is available at: https://pubs.acs.org/10.1021/acsomega.1c03593

Author Contributions

§A.T. and M.T.R. contributed equally to this work.

Author Contributions

A.T. and M.T.R. initiated the project, designed and performed experiments, analyzed data, and wrote the paper. S.P., S.L., T.B.N.N., T.H.N.V., and S.K. analyzed data. T.H.H. and S.H.P. initiated and directed the project, designed experiments, analyzed data, and wrote the paper. The manuscript was written through contributions of all authors. All authors have given approval to the final version of the manuscript.

Funding

This work was supported by KRIBB Research Initiative Programs and the National Research Foundation (NRF) of Korea (2019R1I1A1A01060208, 2021R1A2C1005279, and 2021R1A2C2013879).

Notes

The authors declare no competing financial interest.

■ ABBREVIATIONS

DNA, deoxyribonucleic acid; SP, simulated pattern; OP, observed pattern; EP, experimental pattern; DX, double-crossover; AFM, atomic force microscopy; HPLC, high-performance liquid chromatography; TAE, tris-acetate-EDTA; EDTA, ethylenediaminetetraacetic acid

■ REFERENCES

(1) Zhang, Y.; Seeman, N. C. Construction of a DNA-Truncated Octahedron. *J. Am. Chem. Soc.* **1994**, *116*, 1661−1669.

(2) Winfree, E.; Liu, F.; Wenzler, L. A.; Seeman, N. C. Design and self-assembly of two-dimensional DNA crystals. *Nature* **1998**, *394*, 539−544.

(3) Mao, C.; Sun, W.; Seeman, N. C. Designed Two-Dimensional DNA Holiday Junction Arrays Visualized by Atomic Force Microscopy. *J. Am. Chem. Soc.* **1999**, *121*, 5437−5443.

(4) Mao, C.; LaBean, T. H.; Reif, J. H.; Seeman, N. C. Logical computation using algorithmic self-assembly of DNA triple-crossover molecules. *Nature* **2000**, *407*, 493−496.

(5) LaBean, T. H.; Yan, H.; Kopatsch, J.; Liu, F.; Winfree, E.; Reif, J. H.; Seeman, N. C. Construction, Analysis, Ligation, and Self-Assembly of DNA Triple Crossover Complexes. *J. Am. Chem. Soc.* **2000**, *122*, 1848−1860.
(6) Ding, B.; Sha, R.; Seeman, N. C. Pseudohexagonal 2D DNA Crystals from Double Crossover Cohesion. *J. Am. Chem. Soc.* **2004**, *126*, 10230−10231.
(7) Park, S. H.; Yin, P.; Liu, Y.; Reif, J. H.; LaBean, T. H.; Yan, H. Programmable DNA Self-Assemblies for Nanoscale Organization of Ligands and Proteins. *Nano Lett.* **2005**, *5*, 729−733.
(8) Zheng, J.; Birktoft, J. J.; Chen, Y.; Wang, T.; Sha, R.; Constantinou, P. E.; Ginell, S. L.; Mao, C.; Seeman, N. C. From molecular to macroscopic via the rational design of a self-assembled 3D DNA crystal. *Nature* **2009**, *461*, 74−77.
(9) Hamada, S.; Murata, S. Theoretical model of substrate-assisted self-assembly of DNA nanostructures. *RSC Adv.* **2012**, *2*, 7406−7412.
(10) Tandon, A.; Mitta, S. B.; Vellampatti, S.; Kim, B.; Lee, J.; Kim, S.; Son, J.; Park, S. H. Fabrication of multi-layered DNA nanostructures using single-strand and double-crossover tile connectors. *RSC Adv.* **2015**, *5*, 43234−43241.
(11) Chandrasekaran, A. R.; Zhuo, R. A "tile" tale: Hierarchical self-assembly of DNA lattices. *Appl. Mater. Today* **2016**, *2*, 7−16.
(12) Bhanjadeo, M. M.; Nayak, A. K.; Subudhi, U. Surface-assisted DNA self-assembly: An enzyme-free strategy towards formation of branched DNA lattice. *Biochem. Biophys. Res. Commun.* **2017**, *485*, 492−498.
(13) Lehn, J.-M. Toward complex matter: Supramolecular chemistry and self-organization. *Proc. Natl. Acad. Sci. U.S.A.* **2002**, *99*, 4763−4768.
(14) Wolfram, S. Universality and complexity in cellular automata. *Phys. D* **1984**, *10*, 1−35.
(15) Waddington, C. H.; Cowe, R. J. Computer simulation of a Mulluscan pigmentation pattern. *J. Theor. Biol.* **1969**, *25*, 219−225.
(16) Kusch, I.; Markus, M. Mollusc Shell Pigmentation: Cellular Automaton Simulations and Evidence for Undecidability. *J. Theor. Biol.* **1996**, *178*, 333−340.
(17) Pytte, E.; Grinstein, G.; Traub, R. D. Cellular automaton models of the CA3 region of the hippocampus. *Network* **1991**, *2*, 149−167.
(18) Celada, F.; Seiden, P. E. A computer model of cellular interactions in the immune system. *Immunol. Today* **1992**, *13*, 56−62.
(19) Mallet, D. G.; De Pillis, L. G. A cellular automata model of tumor−immune system interactions. *J. Theor. Biol.* **2006**, *239*, 334−250.
(20) Moreira, J.; Deutsch, A. Cellular automaton models of tumor development: a critical review. *Adv. Complex Syst.* **2002**, *5*, 247−267.
(21) Young, D. A. A local activator-inhibitor model of vertebrate skin patterns. *Math. Biosci.* **1984**, *72*, 51−58.
(22) Xiao, X.; Shao, S.; Ding, Y.; Huang, Z.; Chen, X.; Chou, K.-C. Using cellular automata to generate image representation for biological sequences. *Amino Acids* **2005**, *28*, 29−35.
(23) McKinney, B. A.; Reif, D. M.; Ritchie, M. D.; Moore, J. H. Machine learning for detecting gene-gene interactions: a review. *Appl. Bioinf.* **2006**, *5*, 77−88.
(24) Manukyan, L.; Montandon, S. A.; Fofonjka, A.; Smirnov, S.; Milinkovitch, M. C. A living mesoscopic cellular automaton made of skin scales. *Nature* **2017**, *544*, 173−179.

https://doi.org/10.1021/acsomega.1c03593
ACS Omega 2021, 6, 27038−27044